



UMI-tools: Modelling sequencing errors in Unique Molecular Identifiers to improve quantification accuracy

Tom Sean Smith, Andreas Heger and Ian Sudbery

Genome Res. published online January 18, 2017

Access the most recent version at doi:[10.1101/gr.209601.116](https://doi.org/10.1101/gr.209601.116)

P<P	Published online January 18, 2017 in advance of the print journal.
Accepted Manuscript	Peer-reviewed and accepted for publication but not copyedited or typeset; accepted manuscript is likely to differ from the final, published version.
Open Access	Freely available online through the <i>Genome Research</i> Open Access option.
Creative Commons License	This manuscript is Open Access. This article, published in <i>Genome Research</i> , is available under a Creative Commons License (Attribution 4.0 International license), as described at http://creativecommons.org/licenses/by/4.0/ .
Email Alerting Service	Receive free email alerts when new articles cite this article - sign up in the box at the top right corner of the article or click here .

Advance online articles have been peer reviewed and accepted for publication but have not yet appeared in the paper journal (edited, typeset versions may be posted when available prior to final publication). Advance online articles are citable and establish publication priority; they are indexed by PubMed from initial publication. Citations to Advance online articles must include the digital object identifier (DOIs) and date of initial publication.

To subscribe to *Genome Research* go to:
<https://genome.cshlp.org/subscriptions>

Published by Cold Spring Harbor Laboratory Press

Title

UMI-tools: Modelling sequencing errors in Unique Molecular Identifiers to improve quantification accuracy

Running Title

Modelling UMI errors improves quantification accuracy

Authors

Tom Smith¹

Andreas Heger¹

Ian Sudbery^{2*}

1. Computational Genomics Analysis and Training Programme, MRC WIMM Centre for Computational Biology, University of Oxford, John Radcliffe Hospital/Headley Way, Oxford OX3 9DS

2. Department of Molecular Biology and Biotechnology, University of Sheffield, Firth Court, Western Bank, Sheffield, UK, S10 2TN

* Corresponding author

Keywords

UMI

Unique Molecular Identifier

Random Tag

PCR-duplicates

iCLIP

Single Cell RNA-seq

Sequencing

1 **Abstract**

2 Unique Molecular Identifiers (UMIs) are random oligonucleotide barcodes that are increasingly used
3 in high-throughput sequencing experiments. Through a UMI, identical copies arising from distinct
4 molecules can be distinguished from those arising through PCR-amplification of the same molecule.
5 However, bioinformatic methods to leverage the information from UMIs have yet to be formalised.
6 In particular, sequencing errors in the UMI sequence are often ignored, or else resolved in an *ad-hoc*
7 manner. We show that errors in the UMI sequence are common and introduce network-based
8 methods to account for these errors when identifying PCR duplicates. Using these methods, we
9 demonstrate improved quantification accuracy both under simulated conditions and real iCLIP and
10 single cell RNA-seq datasets. Reproducibility between iCLIP replicates and single cell RNA-seq
11 clustering are both improved using our proposed network-based method, demonstrating the value
12 of properly accounting for errors in UMIs. These methods are implemented in the open source *UMI-*
13 *tools* software package.

14

15 **Background**

16 High throughput sequencing technologies yield vast numbers of short sequences (reads) from a pool
17 of DNA fragments. Over the last ten years a wide variety of sequencing applications have been
18 developed which estimate the abundance of a particular DNA fragment by the number of reads
19 obtained in a sequencing experiment (read counting) and then compare these abundances across
20 biological conditions. Perhaps the most widely used read counting approach is RNA-seq, which seeks
21 to compare the number of copies of each transcript in different cell types or conditions. Prior to
22 sequencing, a PCR amplification step is normally performed to ensure sufficient DNA for sequencing
23 and/or enrichment for fragments with successful adapter ligation. Biases in the PCR amplification
24 step lead to particular sequences becoming overrepresented in the final library (Aird et al. 2011). In
25 order to prevent this bias propagating to the quantification estimates, it is common to remove reads
26 or read pairs with the same alignment coordinates as they are assumed to arise through PCR
27 amplification of the same molecule (Sims et al. 2014). This is appropriate where sequencing depth is
28 low and thus the probability of two independent fragments having the same genomic coordinates
29 are low, as with paired-end whole genome DNA-seq from a large genome. However, the probability
30 of generating independent fragments mapping to the same genomic coordinates increases as the
31 distribution of the alignment coordinates deviates from a random sampling across the genome
32 and/or the sequencing depth increases. For example, in RNA-seq, highly expressed transcripts are
33 more likely to generate multiple fragments with exactly the same genomic coordinates. The problem
34 of PCR duplicates is more acute when greater numbers of PCR cycles are required to increase the
35 library concentration, as in single cell RNA-seq, or when the alignment coordinates are limited to a
36 few distinct loci, as in individual-nucleotide resolution Cross-Linking and ImmunoPrecipitation
37 (iCLIP). Random barcodes were initially proposed as a method to count the number of mRNA
38 molecules in a sample (Hug and Schuler 2003), and have since been used to explicitly label PCR
39 duplicates (McCloskey et al. 2007). More recently, random barcodes, referred to as unique

40 molecular identifiers (UMIs), have been employed to confidently identify PCR duplicates in high-
41 throughput sequencing experiments (König et al. 2010b; Kivioja et al. 2012; Islam et al. 2014). By
42 incorporating a UMI into the same location in each fragment during library preparation, but prior to
43 PCR amplification, it is possible to accurately identify true PCR duplicates as they have both identical
44 alignment coordinates and identical UMI sequences (Figure 1a). In addition to their use in single cell
45 RNA-seq and iCLIP (König et al. 2010b), UMIs may be applied to almost any sequencing method
46 where confident identification of PCR duplicates by alignment coordinates alone is not possible
47 and/or an accurate quantification is required, including ChIP-exo (He et al. 2015), DNA-seq
48 karyotyping (Karlsson et al. 2015), detection of rare mutations (Schmitt et al. 2012) and antibody
49 repertoire sequencing (Vollmers et al. 2013).

50 Accurate quantification with UMIs is predicated on a one-to-one relationship between the number
51 of unique UMI barcodes at a given genomic locus and the number of unique fragments that have
52 been sequenced. However, errors within the UMI sequence including nucleotide substitutions during
53 PCR, and nucleotide miss calling and insertions or deletions (Indels) during sequencing, create
54 additional artefactual UMIs. Nucleotide miss-calling and substitution errors affect only the UMI
55 sequence itself and do not affect the alignment coordinates. Hence, these errors will inflate the
56 estimation of the number of unique molecules at a particular genomic coordinate. These errors can
57 be identified by examining all UMIs at a single genomic coordinate. On the other hand, UMI Indels
58 will affect the alignment position also, leading to the assignment of reads to incorrect genome
59 coordinates. Identification of such events requires the examination of sets of UMIs at neighbouring
60 coordinates. Recombination events, also called 'PCR jumping' create chimeric sequences that may
61 change either the UMI sequence and/or alignment. Miss-calling during sequencing is by far the most
62 prevalent error, occurring 1-2 orders of magnitude more frequently than Indels for Illumina
63 sequencing (Marinier et al. 2015; Schirmer et al. 2015, 2016). Recombination is common when
64 sequencing amplicons, but much rarer with the shotgun sequencing approaches where UMIs are
65 utilised (Schloss et al. 2011; Waugh et al. 2015). We therefore focus here on improving

66 quantification via UMIs by considering nucleotide miss-calling and substitution errors within pools of
67 UMIs from the same genomic coordinate. Herein, we will refer to these errors as UMI errors.

68 UMI errors have been considered in previous analyses (Macosko et al. 2015; Bose et al. 2015; Yaari
69 and Kleinstein 2015; Islam et al. 2014). However, their impact on quantification accuracy has not
70 previously been demonstrated and there is no consistency in the approach taken to resolve these
71 errors. For example, Islam *et al* (2014) removed all UMIs where the counts were below 1 % of the
72 mean counts of all other non-zero UMIs at the genomic locus, whilst Bose *et al* (2015) merged
73 together all UMIs within a hamming distance of two or less, with little explanation as to how this was
74 achieved. We therefore set out to demonstrate the need to account for UMI errors, to compare
75 different methods for resolving UMI errors and to formalise an approach for removing PCR
76 duplicates with UMIs.

77 **Results**

78 We reasoned that UMI errors create groups of similar UMIs at a given genomic locus. To confirm
79 this, we calculated the average number of bases different (edit distance) between UMIs at a given
80 genomic locus and compared the distribution of average edit distances to a null distribution
81 generated by randomly sampling (see methods). Using iCLIP data (Müller-McNicoll et al. 2016), we
82 confirmed that the UMIs are more similar to one another than expected according to the null,
83 strongly suggesting sequencing and/or PCR errors are generating artefactual UMIs (see methods;
84 Figure 1b, see Figure S1 for other datasets). Furthermore, the enrichment of low edit distances is
85 well correlated with the degree of PCR duplication (Figure 1c). Overall, we detected a 25-fold
86 enrichment for positions with an average edit distance of 1, compared to our null expectation. In
87 contrast, when we compared the UMI sequences at adjacent positions we detected an 1.1-fold (+/-
88 standard deviation of 0.1, see materials and methods) enrichment for UMIs which may have
89 originated from a single nucleotide deletion, suggesting UMI Indels are much less prevalent than
90 UMI errors, as expected. We then constructed networks between UMIs at the same genomic locus

91 where nodes represent UMIs and edges connect UMI separated by a single nucleotide difference.
92 Whilst most of the networks contained just a single node, we observed that 3-36% of networks
93 contained two or more nodes, of which 4-20% did not contain a single central node, and thus could
94 not be naively resolved (Figure 1d). This indicates that the majority of networks are likely to
95 originate from a single unique molecule prior to PCR amplification, but a minority of networks may
96 originate from a combination of errors during PCR and sequencing or may originate from multiple
97 unique molecules, which by chance have similar UMIs.

98

99 **Methods to identify unique molecules**

100 Many previous studies assume each UMI at a given genomic locus represents a different unique
101 molecule (Collins et al. 2015; Shiroguchi et al. 2012; Soumillon et al. 2014). We refer to this method
102 as *unique*. Islam *et al* (2014) previously identified the issue of sequencing errors and proposed
103 removing UMIs whose counts fall below a threshold of 1% of the mean of all non-zero UMIs at the
104 locus, a method we refer to as *percentile*.

105 We have developed three methods to identify the number of unique molecules at a given locus by
106 resolving UMI networks formed by linking UMIs separated by a single edit distance (Figure 1e). In all
107 cases, the aim is to reduce the network down to a representative UMI(s) that accounts for the
108 network; identifying the exact sequence of the original UMI(s) is not important for the purposes of
109 quantification. The simplest method we examined was to merge all UMIs within the network,
110 retaining only the UMI with the highest counts. For this method, the number of networks formed at
111 a given locus is equivalent to the estimated number of unique molecules. This is similar to the
112 method employed by Bose et al (2015) where UMIs with an edit distance of 2 or less were
113 considered to originate from an identical molecule. We refer to this method as *cluster*. This method
114 is expected to underestimate the number of unique molecules, especially for complex networks. We

115 therefore developed the *adjacency* method which attempts to correctly resolve the complex
116 networks by using the node counts. The most abundant node and all nodes connected to it are
117 removed from the network. If this does not account for all the nodes in the network, the next most
118 abundant node and its neighbours are also removed. This is repeated until all nodes in the network
119 are accounted for. In the method, the total number of steps to resolve the network(s) formed at a
120 given locus is equivalent to the number of estimated unique molecules. This method allows a
121 complex network to originate from more than one UMI, although UMIs with an edit distance of two
122 will always be removed in separate steps. The excess of UMIs pairs with an edit distance of two
123 observed in the iCLIP datasets indicate that some of these UMIs are artefactual. Reasoning that
124 counts for UMIs generated by a single sequencing error should be higher than those generated by
125 two errors and UMIs resulting from errors during the PCR amplification stage should have higher
126 counts than UMIs resulting from sequencing errors, we developed a final method, *directional*. We
127 generated networks from the UMIs at a single locus, in which directional edges connect nodes a
128 single edit distance apart when $n_a \geq 2n_b - 1$, where n_a and n_b are the counts of node a and node b.
129 The entire directional network is then considered to have originated from the node with the highest
130 counts. The ratio between the final counts for the true UMI and the erroneous UMI generated from
131 a PCR error is dependent upon which PCR cycle the error occurs and the relative amplification
132 biases for the two UMIs, but should rarely be less than 2-fold. The *-1* component was included to
133 account for strings of UMIs with low counts, each separated by a single edit distance for which the
134 $2n$ threshold alone is too conservative. This method allows UMIs separated by edit distances greater
135 than one to be merged so long as the intermediate UMI is also observed, and with each sequential
136 base change from the most abundant UMI, the count decreases. For this method, the number of
137 directional networks formed is equivalent to the estimated number of unique molecules.

138

139

140 Comparing methods with simulated data

141 To compare the accuracy of the proposed methods we simulated the process of UMI amplification
142 and sequencing for UMIs at a single locus and varied the simulation parameters (see methods). To
143 examine the accuracy of the 5 methods, we computed two metrics: The log₂-fold difference
144 between the estimate and ground truth $\text{Log}_2((\text{estimate} - \text{truth}) / \text{truth})$ and the coefficient of
145 variance ($\text{standard deviation} / \text{mean}$) across 10,000 iterations. Increasing UMI length or sequencing
146 depth results in a linear increase in the degree of overestimation for *unique* and *percentile* (Figure
147 2a, b), since increasing either parameter leads linearly increases the total amount of UMI sequence
148 that may harbour errors. In contrast, the estimates from the network-based methods remain
149 relatively stable, with *directional* showing the highest accuracy and lowest variance. We also
150 simulated the effect of including a very long UMI (up to 50 bp) as there may be occasions where it is
151 preferable to concatenate a UMI with another barcode, such as a sample barcode or cell barcode in
152 single cell RNA-seq, leading to longer barcodes. We noted that the network-based methods showed
153 reduced accuracy for very long barcodes (Figure S2a). Investigating further, we found this was
154 correlated with an increase in UMIs with two errors where the single error intermediate was not
155 observed, as detected by counting the number of networks which did not contain any of the initial
156 UMIs prior to PCR and sequencing (Figure S2b). In order to resolve this inherent problem with very
157 long UMIs, we modified the network-based methods so that edges joined nodes with an edit
158 distance less than or equal to 2. This considerably decreased the number of networks without any
159 initial UMIs and improved the accuracy of the network-based methods for very long UMI sequences
160 (Figure S2a-b).

161 Increased sequencing error rate leads to an exponential overestimation for *unique* and *percentile*
162 (Figure 2c), with a 1.3-fold overestimation observed with an error rate of 0.01, compared to less
163 than 1.05-fold for the network based methods. Increasing the rate of errors during the PCR step had
164 a similar impact (Figure S2c). However, this was only observed when the rate of DNA polymerase

165 errors was simulated as greater than 0.001, considerably higher than reported error rates for even
166 non-recombinant *Taq* DNA polymerase (Rittié and Perbal 2008; Whalen et al. 2016), confirming
167 sequencing errors are likely to be the primary source of UMI errors. Increasing the number of PCR
168 cycles or modifying the amplification bias had little impact on the relative accuracy of the methods
169 (Figure S2d, e). Increasing the number of initial UMIs reduced the accuracy of the network-based
170 methods, however even with 100 initial 8bp UMIs at a single locus, the network methods remained
171 the most accurate (Figure S2f).

172 Although the network methods performed very similarly, *directional* consistently yielded more
173 accurate and less variable estimates. For example, when the sequencing depth was increased to 400
174 reads, the average estimates were 19.92, 19.94 and 19.99 (truth=20) respectively for *cluster*,
175 *adjacency* and *directional* methods, and the CVs were 0.0167, 0.0144 and 0.0099. We observed no
176 difference between *percentile* and *unique* under most conditions tested. Increasing the number of
177 reads sequenced per initial UMI, we were able to see an improvement in accuracy for *percentile*
178 relative to *unique* when sequencing error rates are between 1×10^{-3} – 1×10^{-5} , however, even under
179 this specific parameterisation, the network-based methods are more accuracy (Figure S2g).

180 In summary, under simulation conditions, the *directional* method outperforms all other methods,
181 however *adjacency* and *cluster* performs equally well under simulation conditions that are expected
182 to reflect a well-designed experiment and well-executed experiment.

183 **Implementation**

184 To implement our methods within the framework of removing PCR duplicates from BAM alignment
185 files, we developed a command line toolset, UMI-tools, with two commands, *extract* and *dedup*.
186 *extract* takes the UMI from the read sequence contained in a FASTQ read sequence and appends it
187 to the read identifier so it is retained in the downstream alignment. *extract* expects the UMIs to be
188 contained at the same location in each read. Where this is not the case, e.g with sequencing

189 techniques such as inDrop-seq (Klein et al. 2015), the user will need to extract the UMI sequence
190 from the read sequence and append it to the read identifier. *dedup* takes an alignment BAM file,
191 identifies reads with the same genomic coordinates as potential PCR duplicates, and removes PCR
192 duplicates using the UMI sequence according to the method chosen. Time requirements for running
193 *dedup* depend on number of input reads, length of UMI and level of duplication. Memory
194 requirements depend on the number of output reads. On a desktop with a Xeon E3-1246 CPU, it
195 takes ~220 seconds and ~100MB RAM to process a 32 million read single-end input file with 5bp
196 UMIs to ~700,000 unique alignments. Inputs with longer UMIs may take significantly longer.

197

198 **Comparing methods with iCLIP data**

199 We next sought to examine the effect of these methods on real data, starting with the previously
200 mentioned iCLIP data, which includes 3-6 replicates for 9 proteins (Müller-McNicoll et al. 2016). For
201 replicate 1, the distribution of the average edit distance between UMIs present at each genomic
202 locus showed enrichment for single edit distance relative to a null distribution from random
203 sampling, taking into account the genome-wide distribution of UMIs (Figure 3a). For all samples,
204 application of the *directional* method resulted in an edit-distance distribution resembling the null,
205 whereas using the *percentile* method made little or no difference. The same was also true of other
206 replicates of this dataset or other datasets (Figure S2). In some cases a residual enrichment of
207 positions with an average edit distance of 2 was observed, but this was also reduced in most cases.

208 We reasoned that if the *directional* method removed PCR duplicates more accurately, the
209 reproducibility between replicates should be improved. To test this we turned to a previously
210 defined measure of iCLIP reproducibility (König et al. 2010b) . Briefly, we identified in each sample
211 the bases with two or more tags mapping at that positions and asked what percentage had a tag
212 present in one or more other replicates for that pull-down. We limited the analysis to the first three

213 replicates for each protein. In each case, after de-duplication with the *directional* method, bases
214 with two or more tags were more reproducible (Figure 3b), with the difference being very large in
215 some cases (e.g. 21% vs 59% of bases reproducible for SRSF7 replicate 1). In contrast, the *percentile*
216 method was little different from *unique* (Figure S3).

217 In order to measure reproducibility of their data, Müller-McNicoll *et al* measured the spearman's
218 rank correlation between the numbers of significant tags in each exon across the genome. We
219 repeated this calculation with data processed using either the *unique* or *directional* method, and
220 compared the average spearman's correlation between each sample and other replicates of the
221 same pull down. In all cases we see an improvement in the correlation between replicates of the
222 same pull down when data are processed using the *directional* method (Figure 3c). As expected, the
223 degree of improvement for a particular sample was correlated with the enrichment of positions with
224 an average edit distance of 1 (Figure S3; $R^2=0.4$). Thus our method substantially improves the
225 reproducibility of replicates in this iCLIP experiment.

226

227 **Comparing methods with Single Cell RNA Seq data**

228 To further demonstrate the utility of our network-based method, we applied it to two differentiation
229 single cell RNA-seq data sets: the first reported use of UMIs in a single cell RNA-seq experiment
230 seeking to describe a developmental pathway (Soumillon *et al.* 2014), referred to here as SCRB-seq,
231 and a recently reported single cell RNA-seq utilising droplet-barcoding (Klein *et al.* 2015), referred to
232 here as inDrop-seq . As before, network-based methods show a marked improvement in the
233 distribution of edit distances over the *percentile* method and the *unique* method (Figure 4a).
234 Improvements are generally less pronounced than observed with the iCLIP data, likely due to a lower
235 maximum read depth in single cell RNA-seq. To demonstrate that this improvement in the edit
236 distance lead to an improved accuracy in transcript abundance estimates we used the ERCC spike-

237 ins. The naïve use of UMIs to identify PCR duplicates with the *unique* method improved the per-cell
238 correlation between ERCC concentration and counts, compared to quantification without
239 considering PCR duplicates (median coefficients were 0.86 and 0.89, respectively). As expected, the
240 correlation was further improved using the *directional* method (median coefficient = 0.91; Figure
241 4b).

242 We applied hierarchical clustering to the SCRB-seq gene expression data using the *unique* method
243 and observed the Day 0 and Day 14 cells separately relatively well (Figure 4c). However, 7 cells
244 clustered with cells of the wrong time point, reflecting either a failure to commit to differentiation or
245 miss-classification event due to noise in the expression estimates. With the *directional* method this
246 was reduced to 5 cells, suggesting that failure to account for UMI errors can lead to miss-
247 classification in single cell RNA-seq. Applying hierarchical clustering to the the inDrop-seq gene
248 expression estimates, we observed that 44/2717 (1.6%) of cells clustered with cells from another
249 timepoint when using the *unique* method. Biological variation in the progression of differentiation
250 may explain Day 2, Day4 and Day 7 miss-classification events. However, 19/44 events involved
251 undifferentiated mES cells, suggesting these miss-classification events were the result of low-
252 accuracy quantification estimates (Figure 4d). With the application of the *directional* method, the
253 rate of miss-classification was reduced to 0.9% and, strikingly, all the mES cells were correctly
254 classified. These results indicate that application of the *directional* method improves the
255 quantification estimates and can improve classification by hierarchical clustering.

256 **Discussion**

257 UMIs can be utilised across a broad range of sequencing techniques, however bioinformatic
258 methods to leverage the information from UMIs have yet to be standardised. In particular, others
259 have noted the problem of UMI errors, but the solutions applied are varied (Bose et al. 2015; Islam
260 et al. 2014) . The *adjacency* and *directional* methods we set out here are, to our knowledge, novel
261 approaches to remove PCR duplicates when using UMIs. Comparing these methods to previous

262 methods with simulated data, we observed that our methods are superior at estimating the true
263 number of unique molecules. Of the three network-based methods, *directional* was the most robust
264 over the simulation conditions and should be preferred. We note that the performance of all
265 network-based methods will decrease as the number of aligned reads at a genomic locus approaches
266 the number of possible UMIs, however this is an intrinsic issue with UMIs and not one that can be
267 solved computationally post-sequencing. For this reason, we recommend all experiments to use
268 UMIs of at least 8 bp in length and to use longer UMIs for higher sequencing depth experiments. The
269 simulations also indicated that very long UMIs actually decrease the accuracy of quantification when
270 not accounting for UMI errors, since the UMIs are more likely to accumulate errors. For experiments
271 utilising long UMIs, network-based methods therefore show an even greater performance relative to
272 the *unique* method. The simulations provide an insight into the impact on quantification accuracy
273 and indicate that application of an error-aware method is even more important with higher
274 sequencing depth. This is perhaps most pertinent for single cell RNA-seq, as cost decreases continue
275 to drive higher sequencing depths.

276 The analysis of iCLIP and single cell RNA-seq and data sets established that UMI errors present in all
277 of the data sets tested and that quantification accuracy could therefore be improved by modelling
278 these errors during the deduplication step. The frequency of UMI indels was far less than UMI errors
279 suggesting only minimal gains would be achieved by considering UMI indels also. We observed an
280 improved distribution of edit distances for all samples when using network-based methods to detect
281 PCR duplicates, although theoretical reasoning and empirical evidence suggests that the extent of
282 the errors depends on the quality of the sequencing base calls and the sequencing depth, as
283 confirmed by the simulations.

284 Modelling UMI errors yielded improvements in single cell RNA-seq sample clustering, demonstrating
285 the value of considering UMI errors. Since iCLIP aims to identify specific bases bound by RNA binding
286 proteins, datasets have a high level of PCR duplication. The effects of UMI errors are therefore

287 particularly strong, creating the impression of reproducible cross-linking sites within a replicate but
288 not between replicates, for example only 21% of positions with two or more tags in SRSF7 replicate 1
289 had any tags in replicates 2 or 3 when naive de-duplication was used, but this increased to 59%
290 when the *directional* method was used (Figure 3b). Application of the network based methods
291 increases the correlation between replicates in all cases, with larger differences in samples where
292 PCR duplication was higher. From the results of the simulation and real data analyses, we
293 recommend the use of an error-aware method to identify PCR duplicates whenever UMIs are used.

294 We provide our methods within the open-source UMI-tools software
295 (<https://GitHub.com/CGATOxford/UMI-tools>, included here as Supplementary File 1), which can
296 easily be integrated into existing pipelines for analysis of sequencing techniques utilising UMIs.

297

298

299 **Methods**

300 *Simulation*

301 To simulate the effects of errors on UMI counts, an initial number of UMIs were generated at
302 random, with a uniform random probability of amplification [0.8-1.0] assigned to each initial UMI. To
303 simulate a PCR cycle, each UMI was selected in turn and duplicated according to its probability of
304 amplification. Polymerase errors were also added randomly at this stage and any resulting new UMI
305 sequences assigned new probabilities of amplification. Following multiple PCR cycles, a defined
306 number of UMIs were randomly sampled to model the sampling of reads during sequencing
307 (“sequencing depth”) and sequencing errors were introduced with at a given probability, with all
308 errors (e.g A -> T, C -> G) being equally likely. The number of true UMIs within the sampled UMIs was
309 then estimated from the final pool of UMIs using each method. To test the performance of the
310 methods under a variety of simulation parameters, each parameter was varied in turn. The following
311 values are the range of the parameter values tested with the value used for all other simulations in
312 parentheses. Sequencing depth 10-400 (100), number of initial UMIs 10-100 (20), UMI length 6-16
313 (8), DNA polymerase error rate $1 \times 10^{-3} - 1 \times 10^{-7}$ (1×10^{-5}), sequencing error rate $1 \times 10^{-1} - 1 \times 10^{-5}$ ($1 \times$
314 10^{-3}), number of PCR cycles 4-12 (6), minimum amplification probability 0.1-1 (0.8). The maximum
315 amplification probability was set at 1 with the probability of amplification for an each UMI drawn
316 from a uniform distribution.

317

318 **Real data**

319 Re-analysis of the iCLIP and Single Cell RNA-seq data was performed with in-house pipelines
320 following the methods described in the original publication with exceptions as highlighted below.
321 Pipelines are available at https://GitHub.com/CGATOxford/UMI-tools_pipelines and as
322 Supplementary File 2.

323

324 *iCLIP*

325 Raw sequence was obtained from the European Nucleotide Archive (accessions SRP059277 and
326 ERR039854) (Müller-McNicoll et al. 2016; Tollervey et al. 2011). Raw sequences were processed to
327 move the UMI sequences to the read name using 'umi_tools extract'. Sample barcodes were verified
328 and removed, and adaptor sequence removed from the 3' end of reads using the reaper tool from
329 the Kraken package (version 15-065) (Davis et al. 2013) with parameters: '-3p-head-to-tail 2 -3p-
330 prefix 6/2/1'. Reads were mapped to the same genome as the original publication (mm9 for SRSF
331 dataset, hg19 for the TDP43 dataset) using Bowtie version v1.1.2 (Langmead et al. 2009a) with the
332 same parameters as the original publications (-v 2 -m 10 -a).

333 We measured the rate at which UMIs might represent Indel mutations by noting that an Indel in the
334 UMI sequence would cause the final base of the presumed UMI to match the genomic base at
335 position -1 relative to the mapping location of the read. Thus we examined each UMI at a particular
336 position, and tested for the presence of a UMI that would correspond to a 1 bp deletion existed at
337 the following base. We compared this to the situation when the UMIs at the following base were
338 randomised, respecting the number of UMIs at the position and the genome-wide usage of each
339 UMI. Enrichment was defined as the count at the unrandomised positions compared to the count at
340 the randomised positions. We calculated this metric for one replicate of each pull down from
341 SRP059277. See the *Examining_indels* notebook in the *UMI-tools_pipelines* repository (included as
342 Supplementary File 2).

343 Mapped reads were deduplicated using 'umi_tools dedup' using each of the possible methods and
344 edit_distance distribution produced using the '--output-stats' option. For the *cluster* method only the
345 '--further-stats' option was used to output statistics on the distribution of network topology types.

346 Significant bases were produced by comparing tag count height at each position compared to
347 randomised profiles (König et al. 2010a), and bases with $FDR < 0.05$ retained.

348 Coverage over exons was calculated by collapsing Ensembl 67 transcripts. Where exons overlapped,
349 they were restricted to their intersection and the number of reads mapped to significant bases
350 counted for each exon. Exons that contained no tags in any sample were removed (König et al.
351 2010a). Spearman's rho between all pairwise combinations of replicates of pulldowns for the same
352 protein were calculated and averaged for each replicate.

353 Reproducibility between replicates was calculated as per König *et al* (2010). Bases with a depth
354 greater than 2 were identified in the sample in question, and then the fraction of these bases that
355 had one or more tags in other replicates was calculated.

356

357 *Single Cell RNA-seq*

358 For both datasets, raw data was downloaded from Gene Expression Omnibus
359 (<http://www.ncbi.nlm.nih.gov/geo>). For The SCRB-seq data (GSE53638) (Soumillon et al. 2014), a
360 single Day 0 (SRR1058003) and Day 14 (SRR1058023) sample were obtained. For the inDrop data
361 (GSE65525) (Klein et al. 2015), the mouse ES cells sample 1 (SRR1784310), mouse ES cells LIF-, 2 days
362 (SRR1784313), mouse ES cells LIF-, 4 days (SRR1784314) and mouse ES cells LIF-, 7 days
363 (SRR1784315) samples were obtained. FASTQ files were extracted using SRA toolkit. The sequence
364 read filtering, preparation and alignment differed for the two data sets. In both cases, one of the
365 paired end reads contained adapter barcodes and UMI and the other read pair contained sequence
366 for alignment. In addition, with the inDrop data, the position of the UMI within the read varied
367 depending on the length of the cell barcode. For this reason, for both data sets, the UMIs had to be
368 extracted from the reads with bespoke code rather than using UMI-tools *extract*.

369 For SCRB-seq samples, the UMI was extracted from read 2 and appended onto the read identifier of
370 read 1 to generate a single-end FASTQ. Reads were filtered out if any of the following conditions was
371 not met. Phred sequence quality of all cell barcode bases ≥ 10 and all UMI bases ≥ 30 and cell
372 barcode matched expected cell barcodes. A reference transcriptome was built comprising all human
373 protein-coding genes (Ensembl v75, hg19) and the ERCC spike-ins. Since expression quantification
374 was being performed at the gene level, overlapping transcripts from the same gene were merged so
375 that each gene contained a single transcript covering all exons from all transcripts. Reads were
376 aligned to the reference transcriptome using BWA Aln (Li and Durbin 2009) with the following
377 parameters: “-l 24 -k 2” to set seed length to 24 bp, and mismatches allowed in the seed to 2.

378 For inDrop samples, the cell barcode and UMI were extracted from read 1 and read 2 was written
379 out to a single end FASTQ file with the cell barcode incorporated into the file name and the UMI
380 appended to the read identifier. Only reads containing the adapter sequence (allowing 2
381 mismatches) were retained. For each sample, only reads containing one of the n most abundant cell
382 barcodes were retained, where n was the number of cells in a given sample. The resulting single end
383 reads were filtered using trimmomatic v0.32 (Bolger et al. 2014) with the following options:
384 “LEADING:28 SLIDINGWINDOW:4:20 MINLEN:19” to remove bases with Phred quality scores below
385 28 from the 5' end, scan the reads in 4 bp sliding windows and trim when average quality score falls
386 below 20, and retain all reads at least 19bp in length following trimming. Our alignment procedure is
387 a deviation to the method used by Klein *et al* (2015) which involved alignment of reads to a
388 reference transcriptome containing all transcripts (e.g not collapsed into one gene model), reporting
389 up to 200 alignments per read, and dealing with multi-mapping alignments in a downstream step. As
390 this method was not compatible with our de-duplication method we took a simpler approach. A
391 reference transcriptome was built comprising all mouse protein-coding genes (Ensembl v78, mm10)
392 plus ERCC spike-ins. Since expression quantification was being performed at the gene level,
393 overlapping transcripts from the same gene were merged so that each gene contained a single
394 transcript covering all exons from all transcripts. Reads were aligned to the reference transcriptome

395 with Bowtie v1.1.2(Langmead et al. 2009b) with the following options: “-n1 -l 15 -M 1 --best --strata”
396 to allow one mismatch, set seed length to 15 bp and report only one alignment where multiple
397 “best” alignments were found. The seed length and mismatch parameters were the same as the
398 Klein *et al* (2015) alignment method.

399 Following alignment, de-duplication was performed with UMI-tools dedup with *unique*, *percentile*
400 and *directional* used in turn. Both data sets were generated with sequencing methods which
401 generate reads with different alignment coordinates from the same initial DNA fragment (SCRB-seq,
402 CEL-Seq). De-duplication was therefore performed with the “--per-contig” option so that the UMI
403 and the contig (in this case, gene) rather than the exact alignment coordinates were used to identify
404 duplicate reads. The “--stats-output” and “--further-stats” options were used to generate summary
405 statistics for the alignment files pre and post de-duplication. Gene expression was quantified by
406 counting the number of remaining reads per gene following de-duplication

407

408 *Exploratory gene expression analysis*

409 PCA was performed in R (R Core Team 2015) using the *prcomp* function. Hierarchical clustering was
410 performed in R using the *hclust* function and heatmaps generated using the *heatmap.2* function
411 from the *gplots* package. Clustering was performed using 1 - spearman’s correlation coefficient as
412 the distance measure and “ward.D2” as the clustering method. Since many genes show very low
413 expression in the SCRБ-seq data, the top 100 most highly expressed genes were selected for
414 clustering.

415

416 **Data access**

417 UMI-tools is available from pypi (package: umi_tools) and conda (channel:
418 <https://conda.anaconda.org/toms>, package: umi_tools) or GitHub
419 (<https://GitHub.com/CGATOxford/UMI-tools>). Analyses conducted in this manuscript used version
420 0.2.6 - archived on Zenodo as <https://doi.org/10.5281/Zenodo.165403>, and in Supplementary File 1.
421 Analyses were performed using automated python pipelines. iCLIP specific analyses were completed
422 using the iCLIPlib python library (manuscript in preparation). Figures were created by python
423 pipelines or in Jupyter notebooks using the ggplot2 package (Wickham 2009) unless otherwise
424 noted. All pipelines, notebooks and other code, along with configuration files used are available
425 from the GitHub repository (https://GitHub.com/CGATOxford/UMI-tools_pipelines), archived on
426 Zenodo as <https://doi.org/10.5281/zenodo.215974> and in Supplementary File 2.

427

428

429 **Acknowledgements**

430 This research received no specific grant from any funding agency in the public, commercial, or not-
431 for-profit sectors. T.S and A.H are supported by an MRC programme grant [G1000902]. We thank
432 David Sims and members of CGAT for reviewing the manuscript. We thank the GitHub community
433 for helping us to improve the UMI-Tools codebase.

434 *Author contribution:* T.S and I.S. conceived the study. I.S. implemented the first iteration of
435 UMI-Tools. T.S. implemented further methods and improved the code base. A.H implemented
436 performance improvements to UMI-Tools and advised on software development. T.S. performed
437 the simulation and single cell RNA-seq analyses. I.S. performed the iCLIP analysis. T.S and I.S wrote
438 the original draft of the manuscript. T.S, I.S and A.H edited the final draft of the manuscript. I.S.
439 supervised the study.

440

441 **Disclosure Declaration**

442 The authors declare that we have no competing interests

443

References

- Aird D, Ross MG, Chen W-S, Danielsson M, Fennell T, Russ C, Jaffe DB, Nusbaum C, Gnirke A. 2011. Analyzing and minimizing PCR amplification bias in Illumina sequencing libraries. *Genome Biol* **12**: R18.
- Bolger AM, Lohse M, Usadel B. 2014. Trimmomatic: A flexible trimmer for Illumina sequence data. *Bioinformatics* **30**: 2114–2120.
- Bose S, Wan Z, Carr A, Rizvi AH, Vieira G, Pe'er D, Sims P a. 2015. Scalable microfluidics for single cell RNA printing and sequencing. *Genome Biol* **16**: 120.
- Collins JE, Wali N, Sealy IM, Morris JA, White RJ, Leonard SR, Jackson DK, Jones MC, Smerdon NC, Zamora J, et al. 2015. High-throughput and quantitative genome-wide messenger RNA sequencing for molecular phenotyping. *BMC Genomics* **16**: 578.
- Davis MPA, van Dongen S, Abreu-Goodger C, Bartonicek N, Enright AJ. 2013. Kraken: A set of tools for quality control and analysis of high-throughput sequence data. *Methods* **63**: 41–49.
- He Q, Johnston J, Zeitlinger J. 2015. ChIP-nexus enables improved detection of in vivo transcription factor binding footprints. *Nat Biotechnol* **33**: 395–401.
- Hug H, Schuler R. 2003. Measurement of the number of molecules of a single mRNA species in a complex mRNA preparation. *J Theor Biol* **221**: 615–624.
- Islam S, Zeisel A, Joost S, La Manno G, Zajac P, Kasper M, Lönnerberg P, Linnarsson S. 2014. Quantitative single-cell RNA-seq with unique molecular identifiers. *Nat Methods* **11**: 163–6.
- Karlsson K, Sahlin E, Iwarsson E, Westgren M, Nordenskjöld M, Linnarsson S. 2015. Amplification-free sequencing of cell-free DNA for prenatal non-invasive diagnosis of chromosomal aberrations. *Genomics* **105**: 150–8.

- Kivioja T, Vähärautio A, Karlsson K, Bonke M, Enge M, Linnarsson S, Taipale J. 2012. Counting absolute numbers of molecules using unique molecular identifiers. *Nat Methods* **9**: 72–4.
- Klein AM, Mazutis L, Akartuna I, Tallapragada N, Veres A, Li V, Peshkin L, Weitz DA, Kirschner MW. 2015. Droplet Barcoding for Single-Cell Transcriptomics Applied to Embryonic Stem Cells. *Cell* **161**: 1187–1201.
- König J, Zarnack K, Rot G, Curk T, Kayikci M, Zupan B, Turner DJ, Luscombe NM, Ule J. 2010a. iCLIP reveals the function of hnRNP particles in splicing at individual nucleotide resolution. *Nat Struct Mol Biol* **17**: 909–915.
- König J, Zarnack K, Rot G, Curk T, Kayikci M, Zupan B, Turner DJ, Luscombe NM, Ule J. 2010b. iCLIP reveals the function of hnRNP particles in splicing at individual nucleotide resolution. *Nat Struct Mol Biol* **17**: 909–15.
- Langmead B, Trapnell C, Pop M, Salzberg SL. 2009a. Ultrafast and memory-efficient alignment of short DNA sequences to the human genome. *Genome Biol* **10**: R25.
- Langmead B, Trapnell C, Pop M, Salzberg SL. 2009b. Ultrafast and memory-efficient alignment of short DNA sequences to the human genome. *Genome Biol* **10**: R25.
- Li H, Durbin R. 2009. Fast and accurate short read alignment with Burrows-Wheeler transform. *Bioinformatics* **25**: 1754–1760.
- Macosko EZ, Basu A, Satija R, Nemesh J, Shekhar K, Goldman M, Tirosh I, Bialas AR, Kamitaki N, Martersteck EM, et al. 2015. Highly Parallel Genome-wide Expression Profiling of Individual Cells Using Nanoliter Droplets. *Cell* **161**: 1202–1214.
- Marinier E, Brown DG, McConkey BJ. 2015. Pollux: platform independent error correction of single and mixed genomes. *BMC Bioinformatics* **16**: 10.
- McCloskey ML, St??ger R, Hansen RS, Laird CD. 2007. Encoding PCR products with batch-stamps and

barcodes. *Biochem Genet* **45**: 761–767.

Müller-McNicoll M, Botti V, de Jesus Domingues AM, Brandl H, Schwich OD, Steiner MC, Curk T, Poser I, Zarnack K, Neugebauer KM. 2016. SR proteins are NXF1 adaptors that link alternative RNA processing to mRNA export. *Genes Dev* **30**: 553–66.

R Core Team. 2015. R: A Language and Environment for Statistical Computing.

Rittié L, Perbal B. 2008. Enzymes used in molecular biology: A useful guide. *J Cell Commun Signal* **2**: 25–45.

Schirmer M, D'Amore R, Ijaz UZ, Hall N, Quince C. 2016. Illumina error profiles: resolving fine-scale variation in metagenomic sequencing data. *BMC Bioinformatics* **17**: 125.

Schirmer M, Ijaz UZ, D'Amore R, Hall N, Sloan WT, Quince C. 2015. Insight into biases and sequencing errors for amplicon sequencing with the Illumina MiSeq platform. *Nucleic Acids Res* **43**: 1–16.

Schloss PD, Gevers D, Westcott SL. 2011. Reducing the effects of PCR amplification and sequencing artifacts on 16s rRNA-based studies. *PLoS One* **6**.

Schmitt MW, Kennedy SR, Salk JJ, Fox EJ, Hiatt JB, Loeb LA. 2012. Detection of ultra-rare mutations by next-generation sequencing. *Proc Natl Acad Sci* **109**: 14508–14513.

Shiroguchi K, Jia TZ, Sims PA, Xie XS. 2012. Digital RNA sequencing minimizes sequence-dependent bias and amplification noise with optimized single-molecule barcodes. *Proc Natl Acad Sci U S A* **109**: 1347–52.

Sims D, Sudbery I, Ilott NE, Heger A, Ponting CP. 2014. Sequencing depth and coverage: key considerations in genomic analyses. *Nat Rev Genet* **15**: 121–32.

Soumillon M, Cacchiarelli D, Semrau S. 2014. Characterization of directed differentiation by high-throughput single-cell RNA-seq. *BioRxiv*.

- Tollervey JR, Curk T, Rogelj B, Briese M, Cereda M, Kayikci M, Hortobágyi T, Nishimura AL, Župunski V, Patani R, et al. 2011. Characterising the RNA targets and position-dependent splicing regulation by TDP-43; implications for neurodegenerative diseases. *Nat Neurosci* **14**: 452–8.
- Vollmers C, Sit R V, Weinstein JA, Dekker CL, Quake SR. 2013. Genetic measurement of memory B-cell recall using antibody repertoire sequencing. *Proc Natl Acad Sci U S A* **110**: 13463–8.
- Waugh C, Cromer D, Grimm A, Chopra A, Mallal S, Davenport M, Mak J. 2015. A general method to eliminate laboratory induced recombinants during massive, parallel sequencing of cDNA library. *Virology* **12**: 55.
- Whalen S, Truty RM, Pollard KS. 2016. Enhancer-promoter interactions are encoded by complex genomic signatures on looping chromatin. *Nat Genet* **48**: 488–96.
- Wickham H. 2009. *ggplot2: Elegant Graphics for Data Analysis*. Springer-Verlag, New York.
- Yaari G, Kleinstein SH. 2015. Practical guidelines for B-cell receptor repertoire sequencing analysis. *Genome Med* **7**: 121.

Figure Legends

445 **Figure 1. Modelling errors in UMIs**

446 **A.** Schematic representation of how UMIs are used to count unique molecules. Fragmented DNA is
447 labelled with a random UMI sequence (short oligonucleotide; represented as coloured blocks).
448 Following PCR amplification, sequencing and bioinformatics steps, the sequence read alignment
449 coordinates and UMI sequences are used to identify sequence reads originating from the same initial
450 DNA fragment (PCR duplicates) and so count the unique molecules. **B.** Average edit distances
451 (rounder to integers) between UMIs with the same alignment coordinates. Genomic positions with a
452 single UMI are not shown. Null = Null expectation from random sampling of UMIs, taking into
453 account the genome-wide distribution of UMIs. **C.** Correlation between duplication rate and
454 enrichment of positions with an average edit distance of 1 for iCLIP data. **D.** Topologies of networks
455 formed by joining reads with the same genomic coordinates and UMIs a single edit distance apart.
456 Single hub = One node connected to all other nodes. Complex = No node connected to all other
457 nodes. **E.** Methods for estimating unique molecules from UMI sequences and counts at a single
458 locus. Where the method uses the UMI counts, these are shown. Red bases are inferred to be
459 sequencing errors, blue bases inferred to be PCR errors. The inferred number of unique molecules
460 for each method is shown in parentheses.

461 **Figure 2. Comparison of methods with simulated data**

462 In each panel, all but one of the simulation parameters are held constant, with the remaining
463 parameter varied as shown on the x-axis. **A.** UMI length. **B.** Sequencing depth. **C.** Sequencing error
464 rate. Left plot shows the accuracy of quantification, presented as the log₂-transformed normalised
465 difference between the estimate and ground truth. Right plot shows the coefficient of variation
466 (standard deviation / mean). The dashed red line represents the value used for this parameter in all

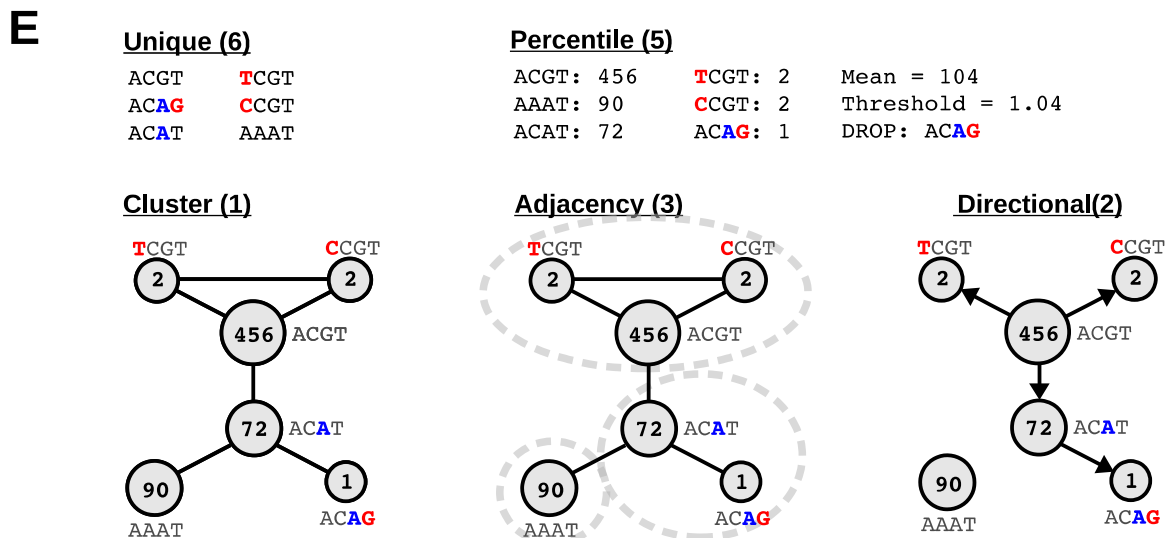
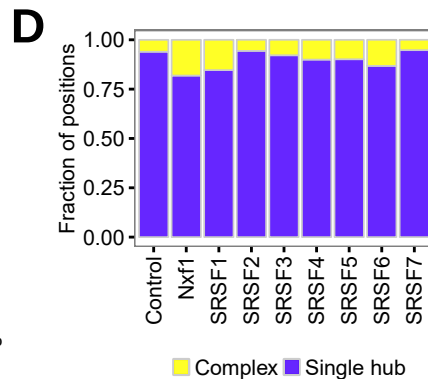
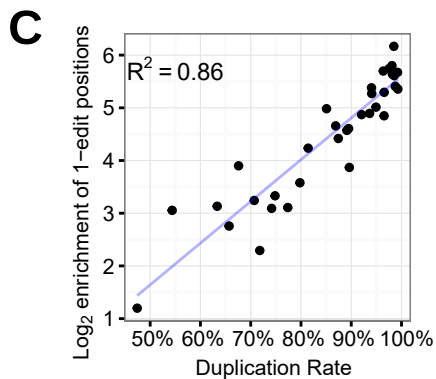
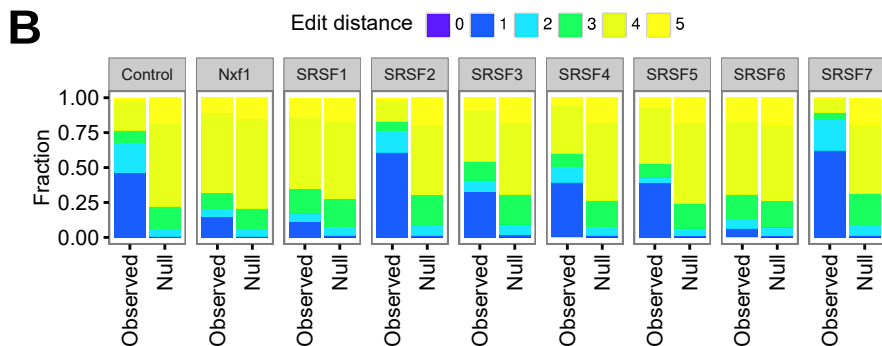
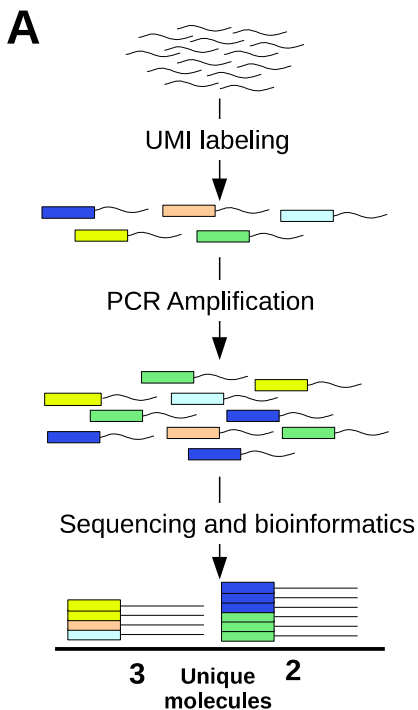
467 other simulations. The dashed grey line represents perfect accuracy. The *unique* and *percentile*
468 methods give identical results with the parameters shown here and are hence overplotted.

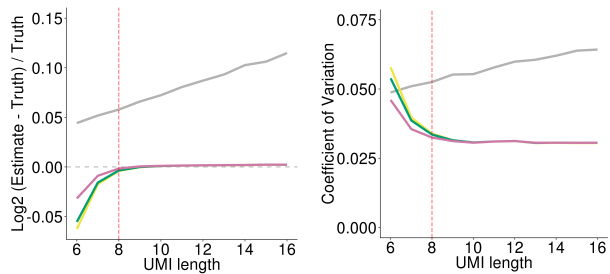
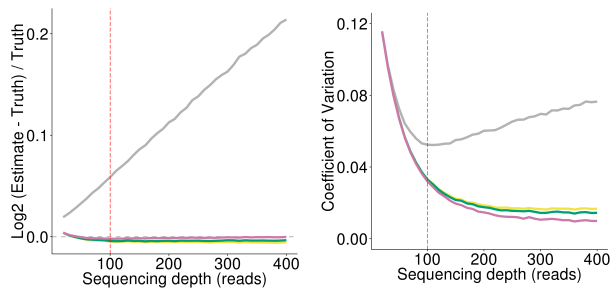
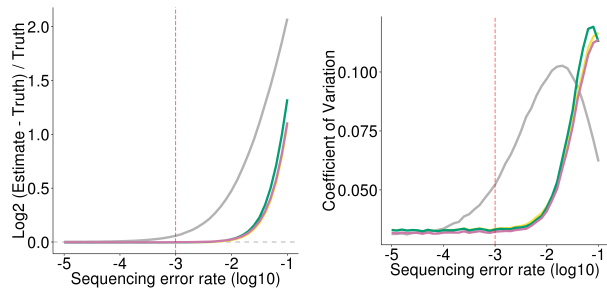
469 **Figure 3. UMI-Tools improves reproducibility between iCLIP replicates**

470 **A.** Average edit distances between UMIs with the same alignment coordinates. Genomic positions
471 with a single UMI are not shown. Null = Null expectation from random sampling of UMIs, taking into
472 account the genome-wide distribution of UMIs. Only the first replicate of the dataset is shown for
473 each pull down **B.** iCLIP reproducibility as represented by the percentage of positions with >2 tags
474 also cross-linked in at least one of 2 other replicates. **C.** Spearman's rank correlation between the
475 numbers of significant tags in each exon

476 **Figure 4. UMI tools improves accuracy and clustering in Single Cell RNA-seq**

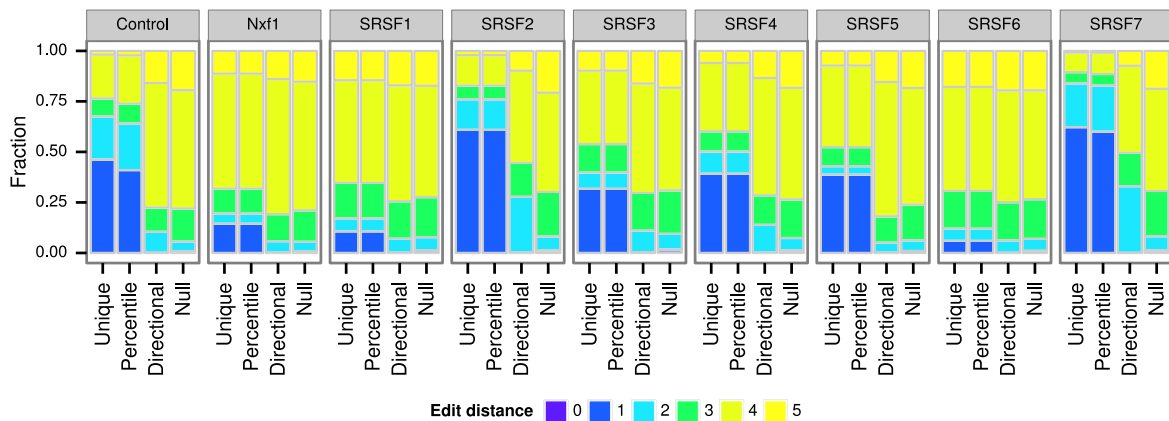
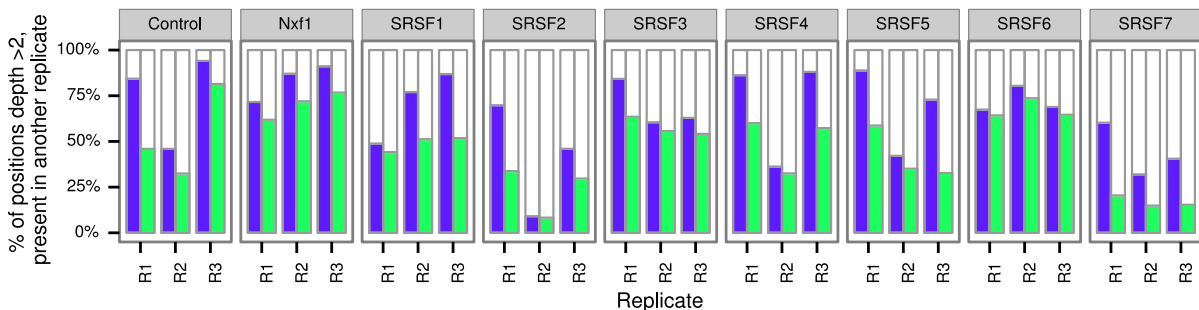
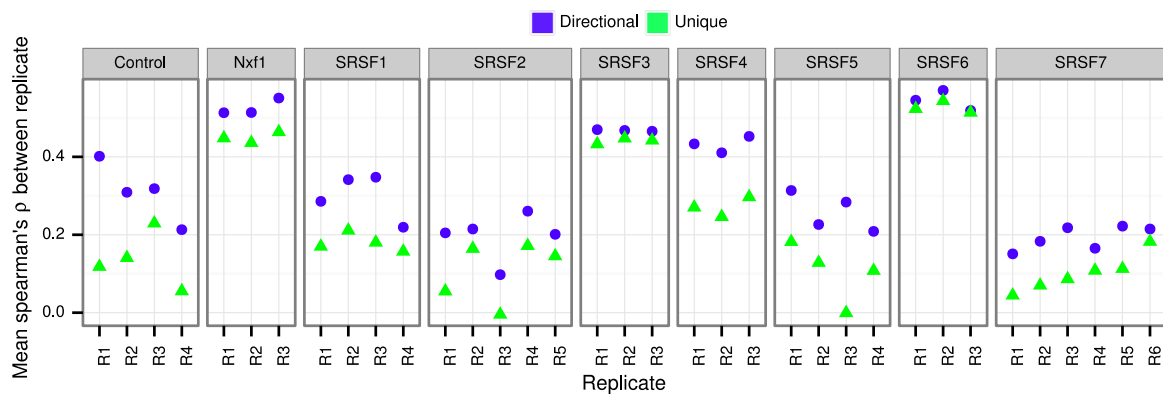
477 **A.** Average edit distances between UMIs with the same alignment coordinates following removal of
478 PCR duplicates using the methods indicated on the x-axis. Genomic positions with a single UMI are
479 not shown. Null: Null expectation from random sampling of UMIs, taking into account the genome-
480 wide distribution of UMIs. Top = SCRB-seq. Bottom = inDrop-seq. **B.** Distribution of pearson
481 correlation coefficients between log ERCC concentration and log counts for raw reads (UMIs
482 ignored) and *unique* and *directional* methods. **C** & **D.** Hierarchical clustering based on the gene
483 expression estimates obtained using *unique* and *directional* Colour bars represent differentiation
484 stage. **C.** SCRB-seq. **D.** inDrop-DSeq. Red arrow indicates mES Cells clustering with Day 4 cells.

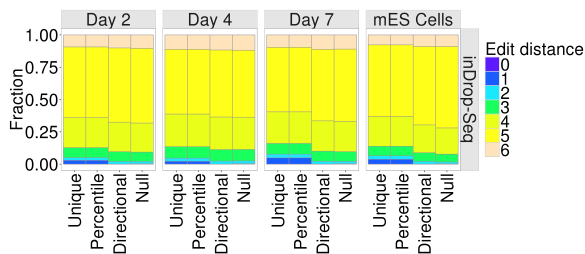
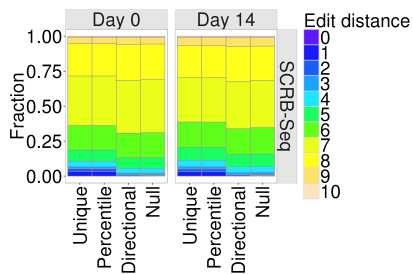
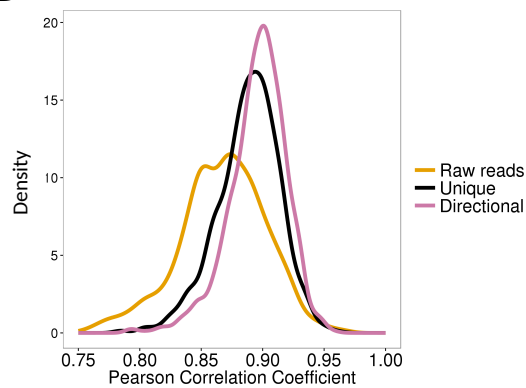
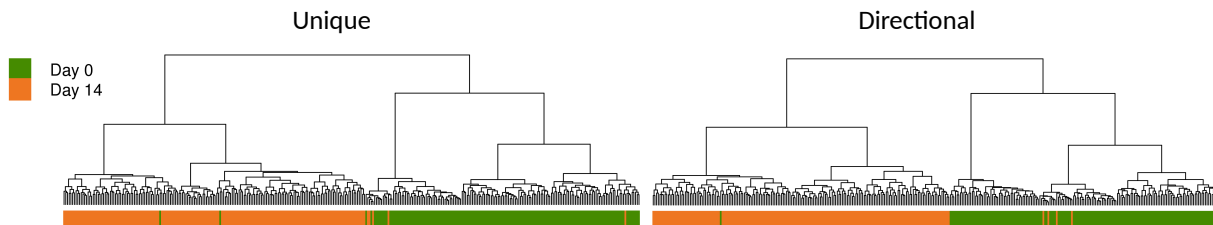


A**B****C**

Method

- Unique
- Percentile
- Cluster
- Adjacency
- Directional

A**B****C**

A**B****C****D**